Quantum Dot-Based Local Field Imaging Reveals Plasmon-Based Interferometric Logic in Silver Nanowire Networks

Hong Wei,[†] Zhipeng Li,[†] Xiaorui Tian,[†] Zhuoxian Wang,[†] Fengzi Cong,[†] Ning Liu,[†] Shunping Zhang,[†] Peter Nordlander,*,[†,‡] Naomi J. Halas,*,[†,§] and Hongxing Xu*,[†,‖]

[†]Beijing National Laboratory for Condensed Matter Physics and Institute of Physics, Chinese Academy of Sciences, Box 603-146, Beijing 100190, China

[‡]Department of Physics and Astronomy, Rice University, MS 61, Houston, Texas 77005, United States

[§]Department of Electrical and Computer Engineering, Rice University, 6100 Main Street, MS-366, Houston, Texas 77005, United States

[‖]Division of Solid State Physics/The Nanometer Structure Consortium, Lund University, Box 118, S-22100, Lund, Sweden

Ⓢ *Supporting Information*

ABSTRACT: We show that the local electric field distribution of propagating plasmons along silver nanowires can be imaged by coating the nanowires with a layer of quantum dots, held off the surface of the nanowire by a nanoscale dielectric spacer layer. In simple networks of silver nanowires with two optical inputs, control of the optical polarization and phase of the input fields directs the guided waves to a specific nanowire output. The QD-luminescent images of these structures reveal that a complete family of phase-dependent, interferometric logic functions can be performed on these simple networks. These results show the potential for plasmonic waveguides to support compact interferometric logic operations.

KEYWORDS: Plasmon, silver nanowire, network, logic, interference, local field distribution
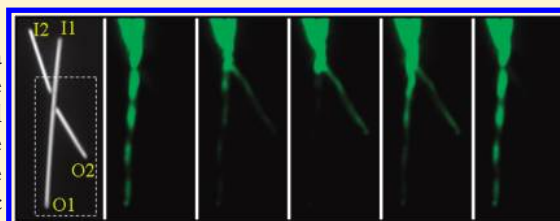
Light-based devices have been proposed for some time as a potential strategy for advancing semiconductor-based computing beyond the fundamental performance limitations of electronic devices, as epitomized by Moore's law.[1−6] Two major classes of all-optical logic have been demonstrated: one based on linear optical effects, known as interferometric logic,[3−9] and the other based on nonlinear optical effects, arising typically from light-induced modulations in the refractive index of an active medium.[1−3] Since interferometric logic depends on the relative optical phase of the two input signals, it manifests inherent stability challenges,[10−13] which may be possible to reduce by device miniaturization and monolithic integration.[7] The diffraction limit of light presents a fundamental obstacle for reducing the dimensions of optical logic components to length scales commensurate with electronic devices in integrated circuits. The coupling of light to surface plasmons (SPs), the collective oscillations of electrons in metallic structures, makes it possible to reduce the dimensions of light-based devices to the nanoscale.[14−20] A wide range of plasmon-based functions important for the development of plasmonic circuitry have recently been demonstrated, such as waveguiding,[21−26] gain,[27−29] electrical excitation[30,31] routing,[32] modulation,[33−36] and detection.[37,38]

In this letter, we report an imaging strategy based on quantum-dot luminescence, that allows us to visualize the near-field distribution of surface plasmons propagating on silver nanowires (NWs) in detail. This provides a valuable tool for the study of plasmons propagating along branched or joined nanowires, forming nanowire networks. In silver nanowire networks of simple geometries, plasmons launched

along a nanowire can be controllably routed to a specific nanowire output. The underlying physical mechanism, interference between SPs launched at different positions along a primary nanowire, is clearly observable, as is the detailed evolution of the plasmon field along the device. The addition of a second plasmon input makes it possible to turn on or off emission paths, resulting in combinations of optical signals that execute specific interferometric Boolean logic operations. These findings shed new light onto our fundamental understanding of propagating plasmons in complex networks and may advance the development of integrated plasmonic devices for new generation information technologies.

Chemically synthesized Ag NWs with smooth surfaces[39] are excellent waveguides that support propagating SPs.[40−42] With the electromagnetic (EM) field strongly confined in the radial direction, light emission from a nanowire occurs only at the ends of the structure. The presence of a symmetry-breaking element, such as an adjacent nanoparticle, a structural anomaly, even the tip of a scanning near-field optical microscope (SNOM), can redirect the emission to other locations.[22,25,43] Here, CdSe@ZnS quantum dots (QDs), separated from the nanowire by a 30 or 50 nm thick Al_2O_3 layer, act as a continuous layer of local reporters of the nanowire evanescent field. Excitation of the QDs is proportional to the local electric field intensity, allowing us to clearly visualize the
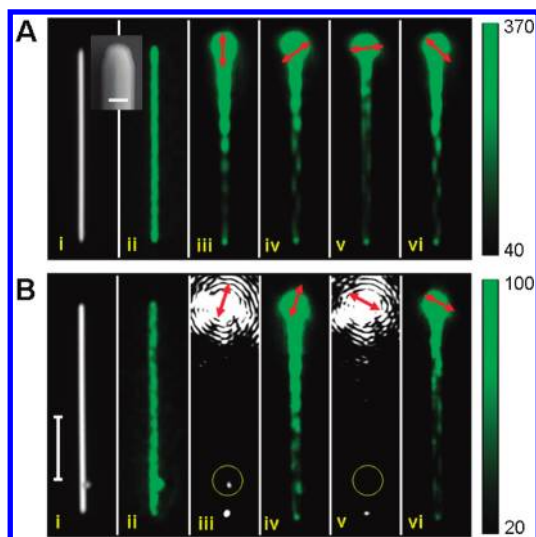
Figure 1. QD emission images of plasmons launched by 632.8 nm laser excitation at one end of a Ag nanowire. Changing the polarization angle at the input modifies the field distribution in the nanowire (A) and controls the emission from an adjacent Ag nanoparticle at the opposite end of the wire (B). (A) (i) Optical image of a NW and a SEM image of a typical NW coated with 30 nm Al_2O_3 (inset). (ii) The QD emission image with wide field excitation. (iii—vi) QD emission images for different incident polarizations. (B) (i) Optical image of a NW-NP system. (ii) The QD emission image with wide field excitation. (iii) Scattering image. (iv) QD emission image corresponding to (iii). (v,vi) Scattering and QD emission images for a different polarization. The scale bar is 200 nm in Ai, and 5 μm in Bi. The red arrows indicate the laser polarization. To enhance the contrast, we use a green color scale to show the intensity distribution of the QD emission. The color scales on the right corresponds to the QD emission images with the excitation light focused on the top ends of the wires.

plasmon-induced field distribution at every point along the entire structure in a minimally perturbative manner. This imaging method enables us to observe the local field distribution in unprecedented detail, providing a clear picture of precisely how plasmons can be redirected by and to additional proximal nanowires at specific points along a primary nanowire.

A bright field image of a typical Ag nanowire and its QD emission image under large-area laser illumination are shown in Figure 1Ai,ii. When a 632.8 nm laser is focused at one end of the nanowire, a periodic nodelike field distribution along the wire is clearly observed (Figure 1Aiii—vi). The large "heads" in the image are caused by the strong QD emission light due to direct focused laser illumination, and the intensity reduction along the nanowire is due to the propagation loss of the nanowire plasmon. The spatial modulation of the near field along the nanowire is a direct result of the interference of the wire plasmons excited by the light source. The excitation light with arbitrary polarization can excite plasmons of different modes, but the spatial distribution of each mode can be quite different. The interference of these modes results in the modulated electric field distribution along the nanowire.[32] The interference pattern is determined by both the relative intensities of the excited modes and their relative phase. The excitation efficiency and thus the magnitude of a certain mode is determined by incident polarization. Therefore the total local field distribution due to constructive or deconstructive interference of different plasmon modes is strongly dependent on the polarization direction of the laser input. For longitudinal incident polarization (Figure 1Aiii), the

near field is distributed symmetrically along the nanowire. Increasing the polarization angle shifts the well-pronounced nodes of the field distribution from one side of the nanowire to the other. This study provides direct and detailed near-field images of how the field distribution of nanowire plasmons can be actively controlled by the physical properties of the "input", in this case, the polarization angle of the incident light launching the NW plasmon. (In the Supporting Information Movie S1, control to the local field distribution is demonstrated dynamically.)

When a structural anomaly, such as an adjacent Ag nanoparticle, is present near a node of the nanowire plasmon, it can affect the plasmon field distribution, and bright emission from the plasmon to the far field results. This scenario is shown in the QD emission image of Figure 1B. The strength of the far-field emission at the adjacent nanoparticle is strongly controlled by the local plasmon-induced field distribution. Here, changing the polarization angle of the plasmon-launching laser controls the light emission from the adjacent Ag nanoparticle. Light emission from the nanoparticle can be varied from a maximally emitting "ON" state (Figure 1Biii), when the node of the field distribution is at the particle (Figure 1Biv), to a minimally emitting "OFF" state (Figure 1Bv), when the node is on the opposite side of the nanowire (Figure 1Bvi). The on/off ratio is observed to be as large as 10 here. Since the complete constructive and deconstructive interference of different modes with different wavelengths are hardly to obtain, there is a fundamental limitation for this ratio depending on how the different plasmon modes are excited and propagated. Further investigations for this issue are currently under investigation.

When a second nanowire is placed in close proximity to the primary nanowire, it can serve as a second input from which a plasmon can be independently launched onto the primary structure (Figure 2A). We can describe the behavior of this simple nanowire network as having two input terminals I1 and I2 and one output terminal (O). In our experiments, the laser beam was split into two beams each with its respective polarization tuned independently by half-wave plates; the phase difference between the two beams was controlled using a Babinet-Soleil Compensator (Foctek Photonics) in one of the beam paths. Both the polarization angle and the phase difference between the two excitation beams I1 and I2 control the emission at output O. Changing the relative phase of the excitation field at I1 and I2 for fixed input polarization illustrates this behavior (Figure 2). As the relative phase between I1 and I2 is monotonically increased, the emission intensity at O varies in an oscillatory manner between a maximum and minimum value (Figure 2B). For the specific input polarizations shown in Figure 2, the ratio of maximum to minimum intensity at O can be larger than 10; however, similar oscillatory behavior can be observed for any pair of incident polarization states although the ratio of maximum to minimum intensity at O may be different. This dynamic range makes it straightforward to assign maximum and minimum output intensities as "ON" and "OFF" states.

When the two input fields (1 and 1) individually or collectively result in a maximum (1), this three-terminal structure represents an OR gate. Conversely, either input signal will emit when launched individually but, when launched jointly, may result in a minimum or OFF state (0) when the two input plasmons interfere destructively. In this case, the structure functions as an XOR gate. The QD emission images for these ON and OFF states (Figure 2C) clearly show the underlying interference-based mechanism resulting in the observed output behavior. For the ON state (Figure 2Ci,ii), a periodic, zigzag nodelike field distribution extending to the output
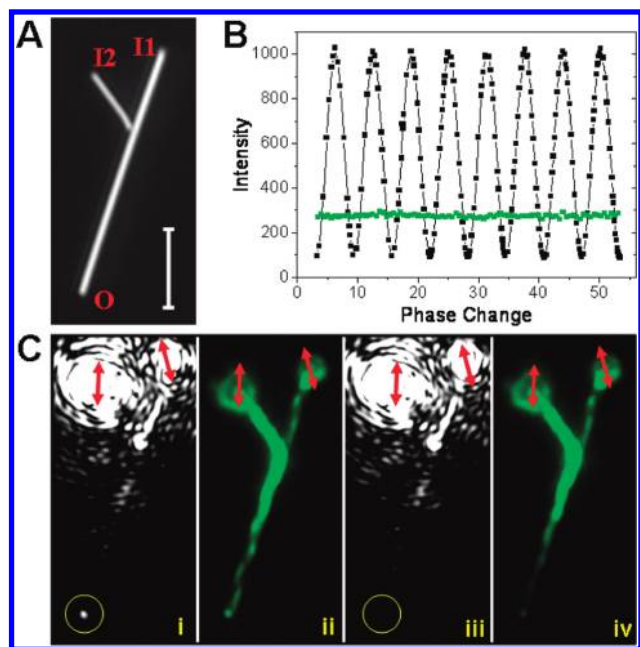
Figure 2. Interference of plasmons in Ag NWs. (A) Optical image of a simple two-nanowire network composed of a primary nanowire and a converging secondary input nanowire. (B) Scattering intensity at output O as a function of optical phase delay when input is either I1 or I2 (green); scattering intensity at output O as a function of optical phase delay for both I1 and I2 inputs (black). (C) (i,iii) Scattering images for the case of two inputs I1 and I2, but with differing phase change. (ii,iv) QD emission images corresponding to i and iii. The red arrows indicate the polarization of the input excitation laser. The Al_2O_3 thickness is 30 nm, and the scale bar is 5 μm.

terminal O is observed when the two propagating plasmons converge onto the primary nanowire of the structure. For the OFF state (Figure 2Ciii,iv), destructive interference of the two input plasmons reduces the field at the output, minimizing light emission (Supporting Information Movie S2). The phase shift is also responsible for the slightly increased attenuation of the propagating plasmon (Figure 2Civ). From these images one can see that the XOR function can also be accomplished by changing the length of the input nanowire of an OR gate by half a wavelength.

By judicious choice of both the input polarization and the relative phase of the excitation laser at the two inputs, plasmon signals can be controlled in different ways. A more complex nanowire network consisting of a primary wire with an additional input and, an additional output is shown in Figure 3A. For this structure, the wire ends marked with I1 and I2 function as inputs while the positions labeled O1 and O2 serve as outputs. For the two incident light polarizations indicated by the red arrows, maximum light emission is varied from O1 and O2 as a function of the relative phase of the two input fields (Figure 3B and Supporting Information Movie S3). This behavior can be understood directly from the QD emission images in Figure 3C (Supporting Information Movie S4). The output from O2 is controlled by the intensity of the field in the wire junction (encircled by the dashed yellow rectangle), and the output from O1 is determined by the field intensity at the end of the primary wire. The O1 and O2 emission intensities over several cycles of relative phase (2π/cycle) of the two inputs is shown in Figure 3D. When the output at O1 is maximal, O2 is close to minimal, and vice versa. The emission data shown in Figure 3D show that the interference between the SPs generated at I1 and I2 is almost ideal. The emission intensity from O1 with input from only
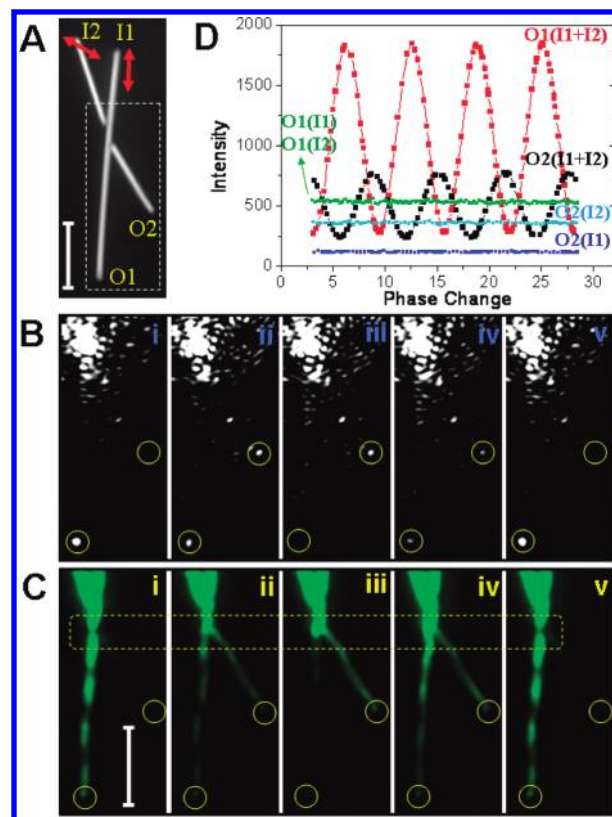
Figure 3. Modulation and routing of light in a two input-two output nanowire network. (A) Optical image of the network. (B) Scattering images for two beam interference in one cycle. (C) QD emission images in one interference cycle. (D) Scattering intensity at O1 and O2 terminals. Red, the intensity of O1 for simultaneous input of both I1 and I2; black, the intensity of O2 for simultaneous input of I1 and I2; green, the intensity of O1 for I1 only and I2 only; cyan, the intensity of O2 for I2 only; blue, the intensity of O2 for I1 only. Al_2O_3 thickness is 50 nm, scale bar is 5 μm. Red arrows in (A) show the polarization of the two laser beams, and the white dashed rectangle in (A) mark the area displayed in (B,C).

I1 or I2 (O1(I1) and O1(I2)) is 500 au. For simultaneous input at I1 and I2 (O1(I1+I2)) the emission from O1 varies from 250 to 1800 au, which is quite close to the 0 to 2000 au range expected for complete destructive and constructive interference. With O2(I1) $\sim$ 100 and O2(I2) $\sim$ 375, complete constructive and destructive interference would result in emission from O2 (O2(I1 + I2)) varying between 90 and 860 au, which is a slightly larger dynamic range than the experimentally observed variation between 250 to 750 au. A phase delay induced by plasmon coupling at the nanowire junction may contribute to this slight asymmetry. Moreover, the O1 and O2 outputs can be modified in additional ways by applying different incident polarizations (see Figure S3, Supporting Information). This combination of polarization and phase control can realize different input-output combinations not achievable by varying only polarization or phase (Supporting Information Figures S4−6 and Movie S5).

By defining specific intensity thresholds for ON and OFF states for the structure in Figure 3, additional logic operations can be realized. For example, for an intensity threshold of 450 au, and considering O2 as the output, (I1 = ON, I2 = OFF) results in O2 = OFF, (I1 = OFF, I2 = ON) results in O2 = OFF, and (I1 = ON, I2 = ON) input results in O2 = ON, demonstrating the behavior of an AND gate.

Table 1. Examples of All-Optical Logic Operations Based on NW Networks[a]

[a] The numbers in red are inputs and the numbers in blue are outputs. Unused terminals are labeled empty. The terminals labeled control require the input to be ON.

A summary of a few of the many logic functions that can be demonstrated in nanowire networks is provided in Table 1. The logic gates AND, OR, and NOT, shown here, are sufficient to realize all binary logic functions. As shown earlier, OR and XOR gates are related to each other, differing at one input by half a plasmon wavelength. Here we also illustrate how the simple network in Figure 3 can be regarded as a binary adder, where two inputs $(1+1)$ result in outputs of 1 (the intensity threshold is defined as >500) at output O2 and 0 at output O1: $1+1 = 10$. Only one above-threshold signal at either input results in 1 at O1 and 0 at O2: $0 + 1 = 1 + 0 = 01$. We also show the schematics of a NAND gate constructed using a network of NWs in a serial AND and NOT configuration.

It is interesting to note that all the plasmonic devices demonstrated here are based on the same principle: interference of plasmons in a primary wire with those introduced by a secondary, adjacent nanowire. This primary wire can thus be viewed as the plasmonic equivalent of a bus in a central processing unit. By loading the primary wire with plasmons launched with specific input properties at the secondary input NWs, the resulting plasmonic interference enables routing and out-coupling to specific output NWs. We believe this concept can be further generalized and expanded to more complex structures that can combine optical signals in various ways, and that a multiple-input, multiple-output plasmonic bus may serve as an efficient splitter, router, switcher and/or multiplexer in future complex plasmonic networks designed for computation and information processing functions. It worthwhile to note that the phase sensitivity of the plasmon structures presented here presents significant challenges for cascaded devices, as one would find in information processing applications. Precise design and fabrication criteria with specific plasmon propagating lengths for phase control would be a necessary requirement for practical plasmon-based interferometric logic. For larger networks, it would likely be necessary to implement amplification schemes using gain media,[27] such as quantum dots or dye molecules, to maintain the signal thresholds required for complex processing functions.

■ ASSOCIATED CONTENT

ⓢ Supporting Information. Detailed experimental materials and methods, QD emission spectrum, SNOM image of the SP in the Ag NW, two-beam interference in four-terminal networks, movies showing the EM near-field distribution or scattering intensity changes corresponding to Figure 1A, Figure 2, Figure 3B, Figure 3C, and Figure S4C. This material is available free of charge via the Internet at http://pubs.acs.org.

■ AUTHOR INFORMATION

Corresponding Author
*E-mail: (H.X.X) hxxu@aphy.iphy.ac.cn; (P.N) nordland@rice.edu; (N.J.H) halas@rice.edu.

■ ACKNOWLEDGMENT

■ REFERENCES

(1) Almeida, V. R.; Barrios, C. A.; Panepucci, R. R.; Lipson, M. *Nature* **2004**, *431* (7012), 1081–1084.

(2) Xu, Q. F.; Lipson, M. *Opt. Express* **2007**, *15* (3), 924–929.

(3) Fainman, Y.; Guest, C. C.; Lee, S. H. *Appl. Opt.* **1986**, *25* (10), 1598–1603.

(4) Kwong, S. K.; Rakuljic, G. A.; Yariv, A. *Appl. Phys. Lett.* **1986**, *48* (3), 201–203.

(5) Ogusu, M.; Tanaka, S.; Kuroda, K. *Jpn. J. Appl. Phys.* **1990**, *29* (7), L1265–L1267.

(6) Zhang, Y. L.; Zhang, Y.; Li, B. J. *Opt. Express* **2007**, *15* (15), 9287–9292.

(7) Caulfield, H. J.; Vikram, C. S.; Zavalin, A. *Optik* **2006**, *117* (5), 199–209.

(8) Qian, L.; Caulfield, H. J. *Inf. Sci.* **2006**, *176* (22), 3379–3392.

(9) Caulfield, H. J.; Soref, R. A.; Vikram, C. S. *Photonics Nanostruct.-Fundam. Appl.* **2007**, *5* (1), 14–20.

(10) Zavalin, A. I.; Shamir, J.; Vikram, C. S.; Caulfield, H. J. *Appl. Opt.* **2006**, *45* (2), 360–365.

(11) Caulfield, H. J.; Dolev, S. *Nat. Photonics* **2010**, *4* (5), 261–263.

(12) Miller, D. A. B. *Nat. Photonics* **2010**, *4* (7), 406–406.

(13) Tucker, R. S. *Nat. Photonics* **2010**, *4* (7), 405–405.

(14) Maier, S. A.; Brongersma, M. L.; Kik, P. G.; Meltzer, S.; Requicha, A. A. G.; Atwater, H. A. *Adv. Mater.* **2001**, *13* (19), 1501–1505.

(15) Fang, N.; Lee, H.; Sun, C.; Zhang, X. *Science* **2005**, *308* (5721), 534–537.

(16) Ozbay, E. *Science* **2006**, *311*, 189–193.

(17) Engheta, N. *Science* **2007**, *317* (5845), 1698–1702.

(18) Polman, A. *Science* **2008**, *322* (5903), 868–869.

(19) Gramotnev, D. K.; Bozhevolnyi, S. I. *Nat. Photonics* **2010**, *4* (2), 83–91.

(20) Brongersma, M. L.; Shalaev, V. M. *Science* **2010**, *328* (5977), 440–441.

(21) Ditlbacher, H.; Hohenau, A.; Wagner, D.; Kreibig, U.; Rogers, M.; Hofer, F.; Aussenegg, F. R.; Krenn, J. R. *Phys. Rev. Lett.* **2005**, *95* (25), No. 257403.

(22) Sanders, A. W.; Routenberg, D. A.; Wiley, B. J.; Xia, Y. N.; Dufresne, E. R.; Reed, M. A. *Nano Lett.* **2006**, *6* (8), 1822–1826.

(23) Yan, R. X.; Pausauskie, P.; Huang, J. X.; Yang, P. D. *Proc. Natl. Acad. Sci. U.S.A.* **2009,** *106* (50), 21045–21050.

(24) Chen, X. W.; Sandoghdar, V.; Agio, M. *Nano Lett.* **2009,** *9* (11), 3756–3761.

(25) Verhagen, E.; Spasenovic, M.; Polman, A.; Kuipers, L. *Phys. Rev. Lett.* **2009,** *102* (20), No. 203904.

(26) Tuchscherer, P.; Rewitz, C.; Voronine, D. V.; de Abajo, F. J. G.; Pfeiffer, W.; Brixner, T. *Opt. Express* **2009,** *17* (16), 14235–14259.

(27) De Leon, I.; Berini, P. *Nat. Photonics* **2010,** *4* (6), 382–387.

(28) Oulton, R. F.; Sorger, V. J.; Zentgraf, T.; Ma, R. M.; Gladden, C.; Dai, L.; Bartal, G.; Zhang, X. *Nature* **2009,** *461* (7264), 629–632.

(29) Noginov, M. A.; Zhu, G.; Belgrave, A. M.; Bakker, R.; Shalaev, V. M.; Narimanov, E. E.; Stout, S.; Herz, E.; Suteewong, T.; Wiesner, U. *Nature* **2009,** *460* (7259), 1110–1112.

(30) Koller, D. M.; Hohenau, A.; Ditlbacher, H.; Galler, N.; Reil, F.; Aussenegg, F. R.; Leitner, A.; List, E. J. W.; Krenn, J. R. *Nat. Photonics* **2008,** *2* (11), 684–687.

(31) Walters, R. J.; van Loon, R. V. A.; Brunets, I.; Schmitz, J.; Polman, A. *Nat. Mater.* **2010,** *9* (1), 21–25.

(32) Fang, Y. R.; Li, Z. P.; Huang, Y. Z.; Zhang, S. P.; Nordlander, P.; Halas, N. J.; Xu, H. X. *Nano Lett.* **2010,** *10* (5), 1950–1954.

(33) Passian, A.; Lereu, A. L.; Arakawa, E. T.; Wig, A.; Thundat, T.; Ferrell, T. L. *Opt. Lett.* **2005,** *30* (1), 41–43.

(34) Dionne, J. A.; Diest, K.; Sweatlock, L. A.; Atwater, H. A. *Nano Lett.* **2009,** *9* (2), 897–902.

(35) Cai, W. S.; White, J. S.; Brongersma, M. L. *Nano Lett.* **2009,** *9* (12), 4403–4411.

(36) MacDonald, K. F.; Samson, Z. L.; Stockman, M. I.; Zheludev, N. I. *Nat. Photonics* **2009,** *3* (1), 55–58.

(37) Falk, A. L.; Koppens, F. H. L.; Yu, C. L.; Kang, K.; Snapp, N. D.; Akimov, A. V.; Jo, M. H.; Lukin, M. D.; Park, H. *Nat. Phys.* **2009,** *5* (7), 475–479.

(38) Neutens, P.; Van Dorpe, P.; De Vlaminck, I.; Lagae, L.; Borghs, G. *Nat. Photonics* **2009,** *3* (5), 283–286.

(39) Sun, Y. G.; Xia, Y. N. *Adv. Mater.* **2002,** *14* (11), 833–837.

(40) Wei, H.; Ratchford, D.; Li, X. Q.; Xu, H. X.; Shih, C. K. *Nano Lett.* **2009,** *9* (12), 4168–4171.

(41) Shegai, T.; Huang, Y. Z.; Xu, H. X.; Kall, M. *Appl. Phys. Lett.* **2010,** *96* (10), No. 103114.

(42) Li, Z. P.; Bao, K.; Fang, Y. R.; Huang, Y. Z.; Nordlander, P.; Xu, H. X. *Nano Lett.* **2010,** *10* (5), 1831–1835.

(43) Knight, M. W.; Grady, N. K.; Bardhan, R.; Hao, F.; Nordlander, P.; Halas, N. J. *Nano Lett.* **2007,** *7*, 2346–2350.